Ab initio study of the $PbTaSe_2$-related superconducting topological metals

Peng-Jen Chen,[1,2,3,*] Tay-Rong Chang,[4] and Horng-Tay Jeng[3,4,†]
[1]*Department of Physics, National Taiwan University, Taipei 10617, Taiwan*
[2]*Nano Science and Technology Program, Taiwan International Graduate Program, Academia Sinica, Taipei 11529, Taiwan and National Taiwan University, Taipei 10617, Taiwan*
[3]*Institute of Physics, Academia Sinica, Taipei 11529, Taiwan*
[4]*Department of Physics, National Tsing Hua University, Hsinchu 30013, Taiwan*
(Received 15 July 2016; published 20 October 2016)

Recent reports have demonstrated the Z_2 topological property of the superconductor $PbTaSe_2$ ($T_c \sim 3.8$ K). $PbTaSe_2$ simultaneously exhibits superconductivity and nontrivial Z_2 topology without the need for doping or proximity effect. Scanning tunneling microscopy confirms that the topological surface states are gapped by superconductivity, indicating the likelihood of the chiral $p_x + ip_y$ pairing mechanism. Motivated by these exciting findings, we predict by means of the first-principles scheme that $ABSe_2$ (A = Pb or Sn and B = Ta or Nb) is also a superconductor with nontrivial Z_2 topology. Among these, $SnNbSe_2$ shows the highest $T_c \sim 7.0$ K. Due to the fact that the required energy resolution to detect the Majorana bound states is of the order of Δ^2/ε_F, the predicted higher T_c of $ABSe_2$ may help mitigate some experimental challenges and provides a better platform for the exploration of the topological superconductivity.

DOI: 10.1103/PhysRevB.94.165148

I. INTRODUCTION

The interplay between superconductivity and nontrivial band topology has gained much attention for its likelihood of realizing the long-sought Majorana fermions [1]. As proposed by Fu and Kane [2,3], two-dimensional (2D) topological superconductivity can be realized on the surface of a topological insulator (TI) placed on top of an s-wave superconductor. Due to the proximity effect, the topological surface states (TSSs) will open up a superconducting gap and hence resemble a system with spinless $p_x + ip_y$ pairing. The Majorana bound states (MBSs) will exist at cores of vortices when applying the magnetic field. In addition to this time-reversal ($\mathcal{T}$) invariant superconducting system, the MBSs can also exist at edges of a superconductor with broken $\mathcal{T}$ that naturally forms $p_x + ip_y$ pairing [4–8]. To date, several works have claimed the observation of superconductivity in topologically nontrivial systems and demonstrated possible signs of nontrivial superconductivity, including the $\mathcal{T}$-invariant Cu- or Sr-doped Bi_2Se_3 [9–13], $Bi_2Se_3/NbSe_2$, and Bi_2Se_3/Bi2212 heterostructures [14–17] and the $\mathcal{T}$-broken system such as ferromagnetic atomic chain deposited on the superconducting surface [18]. In these works of $\mathcal{T}$-invariant systems, the topological materials are turned into a superconducting state by either doping or proximity effect. Stoichiometrical superconductors with nontrivial band topology are still rare; two proposed materials, to our knowledge, are BiPd [19] and β-$PdBi_2$ [20]. Recently, a noncentrosymmetric material $PbTaSe_2$ has been found to be superconducting at temperatures below 3.8 K [21] and soon after its nontrivial topological properties are proposed and confirmed [22,23].

The newly discovered stoichiometrical superconductor $PbTaSe_2$ has been of great interest for it exhibits nontrivial band topology by itself. Without the need of the doping or proximity effect, the TSSs are expected to show a superconducting gap since they cross the Fermi level. The electronic structure, structural stability, superconductivity, and the topological properties of $PbTaSe_2$ have been investigated by Chang *et al.* [22] on the theoretical side. Experimentally, the TSSs have been observed by the scanning tunneling microscopy (STM) and quasiparticle interference (QPI) [23]. The QPI results, combined with the first-principles simulations, confirm the topological character of the surface states. More intriguingly, the STM spectrum reveals a full gap in the superconducting state. That is, the TSSs are gapped by superconductivity as expected. Zero-bias peak is also observed when applying the magnetic field, although better energy resolution is required to gain more decisive evidence for the MBSs. Because the energy spacing of the MBSs is of the order of Δ^2/ε_F (with Δ and ε_F being the superconducting gap and Fermi energy), raising the T_c is helpful for the experimental detection of the MBSs. Thus, superconductors with nontrivial topology and higher T_c are desirable.

In addition to the Z_2 topology, the topological nodal lines (NLs) are also proposed to exist in $PbTaSe_2$ [24]. The topological NLs appear when the touching points of two bands form a closed line in momentum space. Other materials that have been proposed to exhibit NLs include Ca_3P_2 [25,26], Cu_3PdN [27], $TlTaSe_2$ [28], graphene networks [29], and so on. The rich topological nature and superconductivity make $PbTaSe_2$ a promising candidate for further investigation of topological superconductivity.

In this work we employ the first-principles calculations to investigate the electronic structure, superconductivity, and topological properties of the related compounds $ABSe_2$, where A = Pb or Sn and B = Ta or Nb. From our calculations, all the related $ABSe_2$ have higher T_c than $PbTaSe_2$. By comparison, higher T_c is reached when B = Nb, which is possibly because $NbSe_2$ by itself is a superconductor with $T_c \sim 8$ K [30,31] whereas $TaSe_2$ is barely superconducting [32]. Besides, the

*pjchen1015@gate.sinica.edu.tw
†jeng@phys.nthu.edu.tw

topological properties of $ABSe_2$ are also investigated. Despite the smaller spin-orbit coupling (SOC) strength in Sn and Nb, our results indicate that all the $ABSe_2$ compounds under study exhibit nontrivial Z_2 topology. Thus, the related $ABSe_2$ may provide a better platform for the exploration of the exotic topological property in superconducting state because of their higher T_c.

II. COMPUTATIONAL METHODS

The first-principles calculations are performed using QUANTUM ESPRESSO (QE) code [33]. The **k**-meshes used to sample the Brillouin zone (BZ) are $15 \times 15 \times 6$ and $8 \times 8 \times 1$ in the bulk and surface calculations, respectively. A slab consisting of eight layers (unit cells) with both sides terminated at the layer of A atoms is used in surface calculations. The energy cutoff of the plane wave expansion is 40 Ry.

The (electron-) phonon calculations are carried out based on density functional perturbation theory [34] implemented in QE. An $18 \times 18 \times 8$ **k** mesh (for charge density) and a $6 \times 6 \times 4$ **q**-mesh are used in the calculations of phonon spectrum and electron-phonon (e-ph) coupling strength λ:

$$\lambda = \sum_{\mathbf{q}\nu} \lambda_{\mathbf{q}\nu} = \sum_{\mathbf{q}\nu} \frac{1}{\pi N_F} \frac{\Pi''_{\mathbf{q}\nu}}{\omega^2_{\mathbf{q}\nu}}, \tag{1}$$

with ν being the index of phonon modes, N_F the density of states (DOS) at the Fermi level, and Π'' the linewidth of the e-ph quasiparticles. The superconducting T_c is estimated by the McMillan formula:

$$T_c = \frac{\omega_{\ln}}{1.20} \exp\left[-\frac{1.04(1+\lambda)}{\lambda - \mu^*(1+0.62\lambda)}\right] \tag{2}$$

where

$$\omega_{\ln} = \exp\left[\frac{2}{\lambda}\int d\omega \frac{\ln(\omega)}{\omega}\alpha^2 F(\omega)\right]$$

$$\alpha^2 F(\omega) = \frac{1}{2}\int_{BZ} d\omega \lambda_{\mathbf{q}\nu}\omega_{\mathbf{q}\nu}\delta(\omega - \omega_{\mathbf{q}\nu})$$

are the logarithmic average frequency and the isotropic Eliashberg spectrum function, respectively. The screened Coulomb repulsion μ^* is chosen to be 0.1 eV for all materials. The effect of SOC is included in both electronic and phonon calculations.

For computing the Z_2 invariant, the method proposed by Yu *et al.* [35] is adopted. The required Wannier basis is obtained using Wannier90 code [36].

III. RESULTS AND DISCUSSIONS

A. Crystal and electronic structures

The crystal structure of $ABSe_2$ (Fig. 1) is assumed to be identical to that of $PbTaSe_2$ (space group 187: $P\bar{6}m2$). The structure can be viewed as the intercalation of atom A into the layered transition metal dichalcogenide (TMD) BSe_2. The intercalated Pb/Sn sits on top of Se and the original 2H-BSe_2 changes to the AA-stacked structure, making the structure noncentrosymmetric. The relaxed structural parameters of

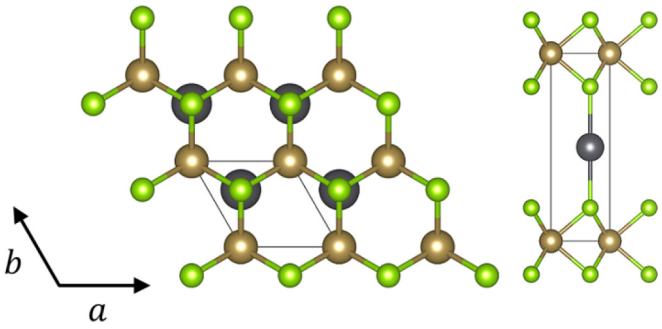

FIG. 1. Top view (left) and side view (right) of $ABSe_2$. The gray, brown, and green spheres represent A, B, and Se atoms, respectively.

$ABSe_2$ are shown in Table I. All these materials have close in-plane lattice constants and show a little variation in c direction, as a result of the different bond lengths between Se and A atoms. Apparently, the A-Se bond length depends on the intercalant. Intercalation of Pb leads to a longer bond length than that of Sn, and hence larger lattice constant in c direction. Also, the A-Se bond lengths are close to the typical values of Pb-Se and Sn-Se bonds, which reveals the three-dimensional (3D) nature of $ABSe_2$.

The band structures with SOC are shown in Fig. 2. Interactions between the A-p and B-d orbitals around the Fermi level are obviously seen, while the states of Se lie away from the Fermi level. These band structures show similar features, with minor distinctions due to the different SOC strengths of Pb and Sn (and possibly Ta and Nb); stronger SOC of Pb opens up a larger gap at K and H points. The SOC, regardless of strength, ensures the existence of a continuous gap over the whole BZ, which is marked by the shaded regions in Fig. 2. The continuous gap, despite the metallicity of these systems, makes the topological Z_2 invariant well defined when counting all bands below it. That is, TSSs that close the continuous gap will exist if the system is topologically nontrivial [20,22,37]. Furthermore, the NLs that have been demonstrated to exist in $PbTaSe_2$ around K and H points are also present in all $ABSe_2$ materials, except that the NL around K seems to be blurred in the Sn-contained systems. Different from $PbTaSe_2$ in which the NLs lie completely above the Fermi level, the NLs in the Sn-contained materials cross the Fermi level. It is then expected that part of the drumhead surface states would be occupied and might exhibit exotic correlation physics [38–40]. The existence of NLs is another

TABLE I. Theoretically relaxed lattice constants and bond lengths ($d_{A\text{-Se}}$ and $d_{A\text{-Se}}$) of $ABSe_2$. All values are displayed in Å. The experimental lattice constants of $PbTaSe_2$ are $a = 3.42$ Å and $c = 9.37$ Å [23].

	lattice constants	$d_{A\text{-Se}}$	$d_{B\text{-Se}}$
$PbTaSe_2$	$a = 3.39$; $c = 9.29$	3.00	2.56
$PbNbSe_2$	$a = 3.41$; $c = 9.26$	2.98	2.56
$SnTaSe_2$	$a = 3.37$; $c = 9.12$	2.90	2.55
$SnNbSe_2$	$a = 3.38$; $c = 9.09$	2.89	2.56

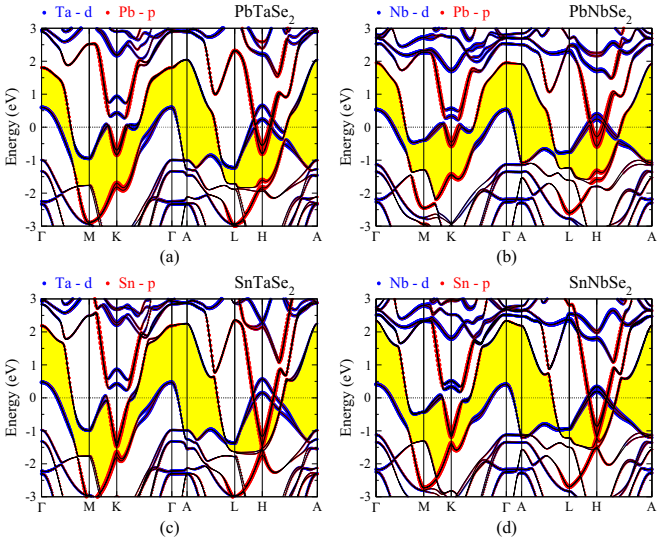

FIG. 2. The bulk band structures of (a) $PbTaSe_2$ (b) $PbNbSe_2$, (c) $SnTaSe_2$, and (d) $SnNbSe_2$. The components of the Pb/Sn-p and Ta/Nb-d orbitals are displayed in red and blue, respectively. The shaded region in each figure indicates the continuous gap below which the corresponding Z_2 invariant is computed.

fascinating topological phenomenon of a different kind but is beyond our purpose in this work. Therefore, we will focus on the Z_2 topology in the following.

B. Phonons and superconductivity

The phonon spectra presented in Fig. 3 confirm the stability of these materials. As discussed in the previous work for $PbTaSe_2$ [26], the originally unstable $TaSe_2$ phonons are pushed upward when intercalated by Pb which suppresses the CDW. The $ABSe_2$ structure is stabilized in a similar fashion; the CDW instability of BSe_2 is suppressed by the intercalation of A atoms, as is revealed by the green and orange bands in the left panel of Fig. 3. Again, these materials exhibit similar phonon spectra, with some energy shifts due to the differences in the atomic masses of the constituents and the subtle e-ph interactions (renormalizations). In addition to the materials under study, we have also investigated combinations of other elements belonging to the same group. It is found that substitutions of vanadium for the B site and/or other lighter IV elements for the A site in $ABSe_2$ incur CDW instability of the structure. For substitution of V, the instability might be attributed to the fact that VSe_2 prefers the 1T to the 1H structure [41–43]. Also, the ferromagnetic ground state of $AVSe_2$ that breaks $\mathcal{T}$ symmetry rules out the possibility of revealing nontrivial Z_2 topology. For the lighter IV elements, the reason for the CDW is possibly due to their shorter bond lengths, e.g., $d_{\text{Ge-Ge}} = 2.38$ Å in germanene [44], as compared with the lattice constant ~3.4 Å of $ABSe_2$. Pressurization or doping might be able to suppress the CDW and induce superconductivity, as is commonly observed in the TMDs [45–47].

The calculated e-ph properties of $ABSe_2$ are shown in Table II. The T_c ranges from 3.1 K of $PbTaSe_2$ to 7.0 K of $SnNbSe_2$. In the previous work for $PbTaSe_2$ [26], the L-phonon (A_{1g} mode) at ~5 meV shows strong e-ph coupling, which is

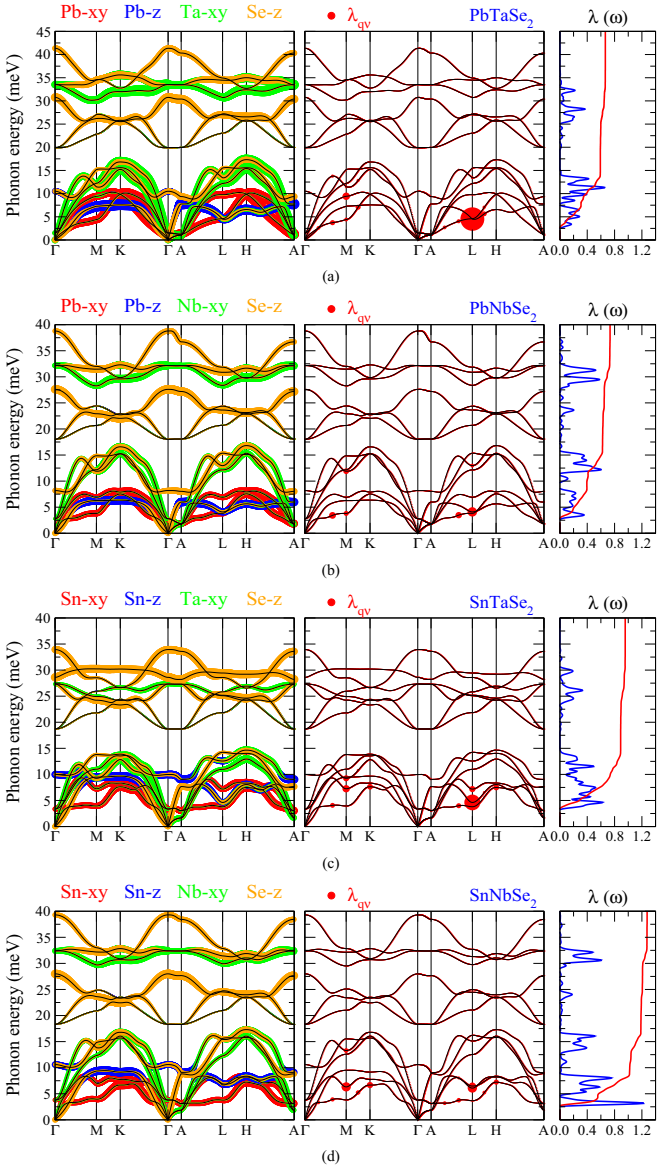

FIG. 3. Phonon spectra, Eliashberg spectrum functions $\alpha^2F(\omega)$, and the integrated e-ph coupling constants $\lambda(\omega)$ of (a) $PbTaSe_2$, (b) $PbNbSe_2$, (c) $SnTaSe_2$, and (d) $SnNbSe_2$. The phonon spectra are displayed with the decomposition of the atomic motions and the magnitudes of $\lambda_{\mathbf{q}\nu}$ (red circles) in left and middle panels, respectively. $\alpha^2F(\omega)$ (blue curve) and $\lambda(\omega) = \int_0^\omega \lambda(\omega')d\omega'$ (red curve) are shown in the right panel. The magnitude of $\lambda_{\mathbf{q}\nu}$, $\alpha^2F(\omega)$, and $\lambda(\omega)$ are displayed with identical scale in all figures for comparison.

also shown in the middle panel of Fig. 3(a). However, the coupling strength decreases rapidly when the phonon wave vector $\mathbf{q}$ moves away from L. Accordingly, the contributions from the low-energy phonons to λ is weakened as shown in $\alpha^2F(\omega)$ where pronounced peaks are absent. Similar behavior is found in $SnTaSe_2$ as well, so this might be thought of as a common property of the $TaSe_2$-based systems. Overall, the $NbSe_2$-based materials have higher T_c than the $TaSe_2$-based ones, and intercalation of Sn leads to higher T_c than that of Pb. By intuition, the former may be understood from the intrinsically higher T_c of $NbSe_2$ than $TaSe_2$, and the latter may be linked with the smaller mass of Sn that yields stronger e-ph

TABLE II. The calculated e-ph properties of $ABSe_2$.

	N_F (states/eV)	$\omega_{\ln}$ (K)	λ	T_c (K)
$PbTaSe_2$	1.64	99.4	0.66	3.1
$PbNbSe_2$	1.90	103.4	0.73	4.0
$SnTaSe_2$	1.46	87.1	0.96	5.7
$SnNbSe_2$	1.58	72.6	1.28	7.0

coupling strength ($\lambda \propto M^{-1}$ via Π''). Phenomenologically, two features of the Eliashberg spectral function $\alpha^2F(\omega)$ are responsible for the difference in T_c. First, there exist two peaks at ~30 meV in the $NbSe_2$-based systems, resulting in a jump in $\lambda(\omega)$. This explains the higher T_c of $PbNbSe_2$ than $PbTaSe_2$. For Sn-intercalated systems, this jump also contributes to the higher T_c of $SnNbSe_2$ but plays a minor role. The second feature is the rapid increase at energies <10 meV in Sn-intercalated systems, giving rise to a larger λ but smaller ω_{ln}. Because of the dominant role of λ over ω_{ln} in the McMillan formula, the Sn-intercalated systems show higher T_c. In addition, a pronounced peak is found in $SnNbSe_2$ at ~3 meV but not (or less obvious) in $SnTaSe_2$. This peak is the main account of the highest T_c of $SnNbSe_2$. In comparison with $SnTaSe_2$, we speculate that the extremely low phonon energy, as well as the high coupling strength, significantly enhances the effect of smaller atomic mass of Nb (compared with Ta) on λ that is inversely proportional to ω^2.

C. Z_2 topological properties

$PbTaSe_2$ has been claimed and confirmed to be a Z_2-nontrivial material [22,23]. Here we are interested in unraveling the topological properties of other $ABSe_2$ compounds. The lack of inversion symmetry in $ABSe_2$ prohibits the applicability of the parity analysis to compute the Z_2 invariant. Several methods have been proposed to deal with the Z_2 invariant of systems without inversion symmetry [35,48–50]. Here we adopt the method proposed by Yu *et al.* [35] to determine the topological phase. It has been proven that the Wanner center is closely related to the Berry curvature [51], so the evolution of the Wannier center is indicative of the Berry phase. Odd (even) winding number of the evolution between two $\mathcal{T}$-invariant momenta indicates nontrivial (trivial) topological state. For 3D materials, the topological phase is determined by two effective 2D systems with $k_z = 0$ and $\frac{\pi}{2}$, respectively. Multiplication of the two Z_2 invariants corresponding to these two effective 2D systems gives the Z_2 of the whole system. As mentioned previously for Z_2 topological metals, the Z_2 invariant of a subsystem containing all bands below the continuous gap is well defined. As shown in Fig. 4 for $ABSe_2$, the winding number is odd at $k_z = 0$ and even at $k_z = \frac{\pi}{2}$, yielding $Z_2 = -1 \cdot 1 = -1$. Therefore, $ABSe_2$ materials are all topologically nontrivial. It is noted that the phase evolution path is closely dependent on the A atom, implying its dominant role in making the system topologically nontrivial.

To make the nontrivial topology more evident, we also carry out the calculations of the surface band structure. Indeed, the surface states crossing the continuous gap are present and

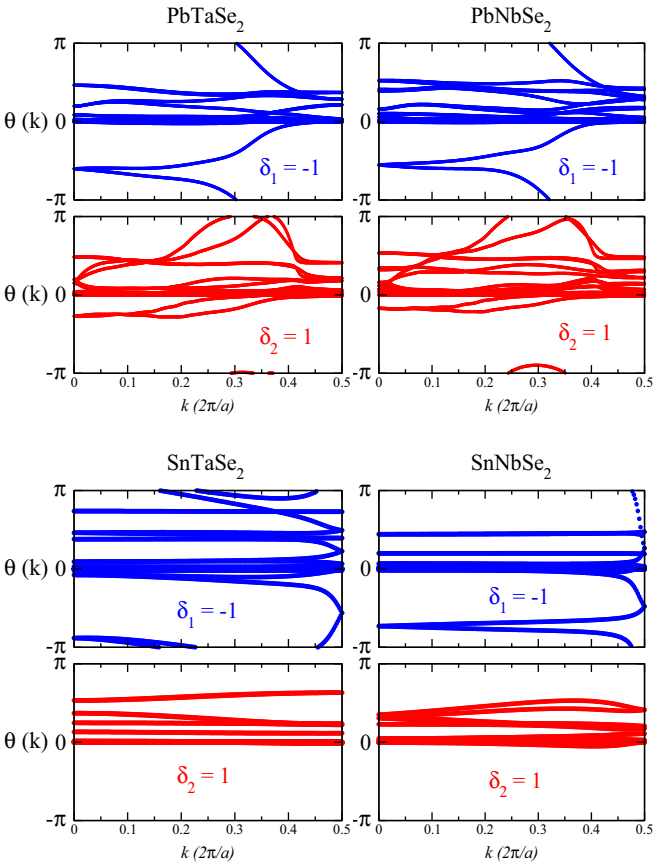

FIG. 4. The phase evolution of the Wannier centers of $ABSe_2$. The left and right panels represent the phase evolution of the effective 2D system at $k_z = 0$ and $\frac{\pi}{2}$, respectively. $Z_2 = \delta_1 \cdot \delta_2 = -1$ for all these materials, indicating the topologically nontrivial state.

degenerate at Γ as revealed in Fig. 5. We would like to emphasize that these two surface states connect two sets of bands which are fully separated in bulk by the continuous gap. The closing of the continuous gap by surface states supports the topological origin. Similar with $PbTaSe_2$, the "Dirac" point, or crossing point (CP), lies about 0.5 eV above the Fermi level. Different from the common CP near which the bands disperse linearly, the vicinity of the CP shows quadratic (or higher order) dependence on **k**. More interesting is that the two branches are both holelike (i.e., no particlelike branch) in this "Dirac" system. It would be interesting and important to discuss the difference between the crossing of topological bands of this kind and the common Dirac system in which both particlelike and holelike branches are present and exhibit linearity in **k**, especially their role played in superconductivity.

The spin-momentum lock, one of the characteristics of a TSS, is clearly depicted by the in-plane components of the spin states shown in Fig. 5. The decomposed $\langle s_y \rangle$ is zero along the direction of y (Γ-M), and $\langle s_x \rangle$ is zero along x (Γ-K). Interestingly, the TSSs in Ta-contained materials show nonzero $\langle s_z \rangle$ components. The canted spin states provide an additional scattering channel between states whose backscattering from in-plane components is forbidden. This additional scattering process due to canted spin is indeed observed in the QPI results of $PbTaSe_2$ [23]. For Nb-contained

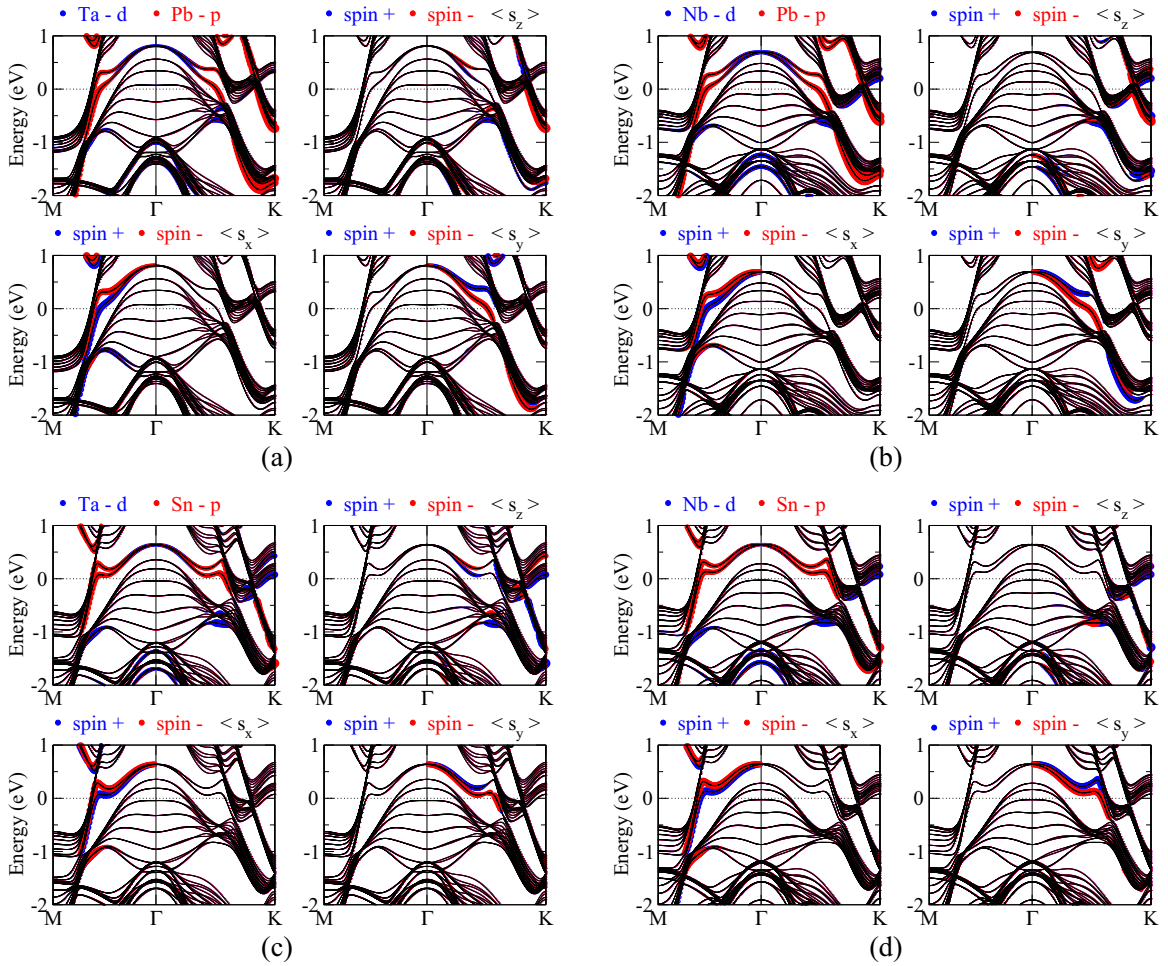

FIG. 5. The decomposed surface band structures of (a) $PbTaSe_2$, (b) $PbNbSe_2$, (c) $SnTaSe_2$, and (d) $SnNbSe_2$. As denoted on top of each panel, projected A-p and B-d orbitals of the surface atoms are shown in the top-left panel in each figure, while the other panels display the projected spin polarizations of bands contributed from the surface atoms. The Γ-K and Γ-M directions are chosen to lie along $+x$ and $+y$, respectively, to clearly demonstrate the behavior of spin-momentum lock.

materials, the spins are found to be nearly in-plane with negligible canting. We speculate that the canting of spins in Ta-contained materials is originated from the larger SOC of Ta that more efficiently couples the three Pauli matrices. The influence of the canted spins on superconductivity pairing is also an essential issue that calls for further investigations.

Noteworthy to mention, β-$PdBi_2$ is recently proposed to be a superconductor that possesses two sets of TSSs [20]. The set with lower energy lies entirely below the Fermi level, so it is irrelevant to the superconductivity. The other set, on the other hand, crosses the Fermi level and is expected to play a role in superconductivity. However, these TSSs in β-$PdBi_2$ severely merge into the bulk states. As revealed in Fig. 5 for $ABSe_2$, the spin helicity disappears when the TSSs are buried inside the bulk bands along Γ-K. As a result, how the bulk states affect the topological character of the TSSs in β-$PdBi_2$ under this condition remains a question. In $ABSe_2$, at least one TSS remains separated from the bulk bands at the Fermi level and preserves the helical spin states, which is important for the $p_x + ip_y$ pairing as proposed by Fu and Kane [2,3]. As for BiPd, the exact computation of Z_2 is lacking. The possibility of being a topologically nontrivial material is inferred from the band crossing observed in the band structure. Since this kind of band crossing is not a unique consequence of nontrivial band topology, its nontrivial topological state requires further study to confirm.

Before closing the discussion, we would like to point out that the T_c of $SnNbSe_2$ is higher than that of the existing superconductors that also show TSSs, such as $PbTaSe_2$ (3.8 K) [21,23], Bi_2Pd (5.3 K) [20], and BiPd (3.8 K) [19]. Therefore, the $ABSe_2$ materials provide a better platform for the investigation of the chiral $p_x + ip_y$ pairing and the detection of MBSs which entails energy resolution of the order of Δ^2/ε_F.

IV. SUMMARY

To sum up, motivated by the exotic properties of the recently discovered superconductor $PbTaSe_2$, we predict by first-principles calculations that $PbNbSe_2$, $SnTaSe_2$, and $SnNbSe_2$ are also superconductors that reveal nontrivial Z_2 topology. Detailed analyses of the electronic structures and e-ph interactions are given to demonstrate and discuss

the superconductivity and topological properties. $SnNbSe_2$ exhibits highest $T_c \sim 7.0$ K in this family. Besides, the TSSs in $ABSe_2$ are separated from the bulk bands and remain unaffected. The preserved helical spin states, as well as the higher T_c, are beneficial for the experimental exploration of the possible chiral p-wave superconducting state and the MBSs.

ACKNOWLEDGMENTS

P. J. Chen thanks fruitful discussions with Ting-Kuo Lee, Tien-Ming Chuang, and Wan-Ju Li. The authors acknowledge National Center for High-Performance Computing (NCHC). This work is supported by the Ministry of Science and Technology, Academia Sinica, National Taiwan University, and National Tsing-Hua University, Taiwan.

[1] E. Majorana, Nuovo Cimento **14**, 171 (1937).
[2] L. Fu and C. L. Kane, Phys. Rev. B **74**, 195312 (2006).
[3] L. Fu and C. L. Kane, Phys. Rev. Lett. **100**, 096407 (2008).
[4] A. Y. Kitaev, Phys. Usp. **44**, 131 (2001).
[5] M. Z. Hasan and C. L. Kane, Rev. Mod. Phys. **82**, 3045 (2010).
[6] X.-L. Qi and S.-C. Zhang, Rev. Mod. Phys. **83**, 1057 (2011).
[7] J. Alicea, Rep. Prog. Phys. **75**, 076501 (2012).
[8] C. W. J. Beenakker, Annu. Rev. Condens. Matter Phys. **4**, 113 (2013).
[9] Y. S. Hor, A. J. Williams, J. G. Checkelsky, P. Roushan, J. Seo, Q. Xu, H. W. Zandbergen, A. Yazdani, N. P. Ong, and R. J. Cava, Phys. Rev. Lett. **104**, 057001 (2010).
[10] K. Matano, M. Kriener, K. Segawa, Y. Ando, and G.-Q. Zheng, Nat. Phys. **12**, 852 (2016).
[11] Shruti, V. K. Maurya, P. Neha, P. Srivastava, and S. Patnaik, Phys. Rev. B **92**, 020506(R) (2015).
[12] Z. Liu, X. Yao, J. Shao, M. Zuo, L. Pi, S. Tan, C. Zhang, and Y. Zhang, J. Am. Chem. Soc. **137**, 10512 (2015).
[13] Y. Pan, A. M. Nikitin, G. K. Araizi, Y. K. Huang, Y. Matsushita, T. Naka, and A. de Visser, Sci. Rep. **6**, 28632 (2016).
[14] J.-P. Xu, M.-X. Wang, Z. L. Liu, J.-F. Ge, X. Yang, C. Liu, Z. A. Xu, D. Guan, C. L. Gao, D. Qian, Y. Liu, Q.-H. Wang, F.-C. Zhang, Q.-K. Xue, and J.-F. Jia, Phys. Rev. Lett. **114**, 017001 (2015).
[15] H.-H. Sun, K.-W. Zhang, L.-H. Hu, C. Li, G.-Y. Wang, H.-Y. Ma, Z.-A. Xu, C.-L. Gao, D.-D. Guan, Y.-Y. Li, C. Liu, D. Qian, Y. Zhou, L. Fu, S.-C. Li, F.-C. Zhang, and J.-F. Jia, Phys. Rev. Lett. **116**, 257003 (2016).
[16] P. Zareapour, A. Hayat, S. Y. F. Zhao, M. Kreshchuk, A. Jain, D. C. Kwok, N. Lee, S.-W. Cheong, Z. Xu, A. Yang, G. D. Gu, S. Jia, R. J. Cava, and K. S. Burch, Nat. Commun. **3**, 1056 (2012).
[17] E. Wang, H. Ding, A. V. Fedorov, W. Yao, Z. Li, Y.-F. Lv, K. Zhao, L.-G. Zhang, Z. Xu, J. Schneeloch, R. Zhong, S.-H. Ji, L. Wang, K. He, X. Ma, G. Gu, H. Yao, Q.-K. Xue, X. Chen, and S. Zhou, Nat. Phys. **9**, 621 (2013).
[18] S. Nadj-Perge, I. K. Drozdov, J. Li, H. Chen, S. Jeon, J. Seo, A. H. MacDonald, B. A. Bernevig, and A. Yazdani, Science **346**, 602 (2014).
[19] Z. Sun, M. Enayat, A. Maldonado, C. Lithgow, E. Yelland, D. C. Peets, A. Yaresko, A. P. Schnyder, and P. Wahl, Nat. Commun. **6**, 6633 (2015).
[20] M. Sakano, K. Okawa, M. Kanou, H. Sanjo, T. Okuda, T. Sasagawa, and K. Ishizaka, Nat. Commun. **6**, 8595 (2015).
[21] M. N. Ali, Q. D. Gibson, T. Klimczuk, and R. J. Cava, Phys. Rev. B **89**, 020505(R) (2014).
[22] T.-R. Chang, P.-J. Chen, G. Bian, S.-M. Huang, H. Zheng, T. Neupert, R. Sankar, S.-Y. Xu, I. Belopolski, G. Chang, B. K. Wang, F. Chou, A. Bansil, H.-T. Jeng, H. Lin, and M. Z. Hasan, Phys. Rev. B **93**, 245130 (2016).
[23] S.-Y. Guan, P.-J. Chen, M.-W. Chu, R. Sankar, F. C. Chou, H.-T. Jeng, C.-S. Chang, and T.-M. Chuang, arXiv:1605.00548.
[24] G. Bian, T. R. Chang, R. Sankar, S. Y. Xu, H. Zheng, T. Neupert, C. K. Chiu, S. M. Huang, G. Chang, I. Belopolski, D. S. Sanchez, M. Neupane, N. Alidoust, C. Liu, B. Wang, C. C. Lee, H. T. Jeng, C. Zhang, Z. Yuan, S. Jia, A. Bansil, F. C. Chou, H. Lin, and M. Z. Hasan, Nat. Commun. **7**, 10556 (2016).
[25] L. S. Xie, L. M. Schoop, E. M. Seibel, Q. D. Gibson, W. Xie, and R. J. Cava, APL Mater. **3**, 083602 (2015).
[26] Y.-H. Chan, C.-K. Chiu, M. Y. Chou, and A. P. Schnyder, Phys. Rev. B **93**, 205132 (2016).
[27] R. Yu, H. Weng, Z. Fang, X. Dai, and X. Hu, Phys. Rev. Lett. **115**, 036807 (2015).
[28] G. Bian, T.-R. Chang, H. Zheng, S. Velury, S.-Y. Xu, T. Neupert, C.-K. Chiu, S. M. Huang, D. S. Sanchez, I. Belopolski, N. Alidoust, P.-J. Chen, G. Chang, A. Bansil, H.-T. Jeng, H. Lin, and M. Z. Hasan, Phys. Rev. B **93**, 121113(R) (2016).
[29] H. Weng, Y. Liang, Q. Xu, R. Yu, Z. Fang, X. Dai, and Y. Kawazoe, Phys. Rev. B **92**, 045108 (2015).
[30] D. Jarome, A. J. Grant, and A. D. Yoffe, Solid State Commun. **9**, 2183 (1971).
[31] R. E. Jones Jr., H. R. Shanks, and D. K. Finnemore, Phys. Rev. B **6**, 835 (1972).
[32] K. Yokota, G. Kurata, T. Matsui, and H. Fukuyama, Physica B: Condens. Matter **284–288**, 551 (2000).
[33] P. Giannozzi, S. Baroni, N. Bonini, M. Calandra, R. Car, C. Cavazzoni, D. Ceresoli, G. L. Chiarotti, M. Cococcioni, I. Dabo, A. Dal Corso, S. de Gironcoli, S. Fabris, G. Fratesi, R. Gebauer, U. Gerstmann, C. Gougoussis, A. Kokalj, M. Lazzeri, L. Martin-Samos, N. Marzari, F. Mauri, R. Mazzarello, S. Paolini, A. Pasquarello, L. Paulatto, C. Sbraccia, S. Scandolo, G. Sclauzero, A. P. Seitsonen, A. Smogunov, P. Umari, and R. M. Wentzcovitch, J. Phys.: Condens. Matter **21**, 395502 (2009).
[34] S. Baroni, S. de Gironcoli, and A. Dal Corso, Rev. Mod. Phys. **73**, 515 (2001).
[35] R. Yu, X.-L. Qi, A. Bernevig, Z. Fang, and X. Dai, Phys. Rev. B **84**, 075119 (2011).
[36] A. A. Mostofi, J. R. Yates, G. Pizzi, Y. S. Lee, I. Souza, D. Vanderbilt, and N. Marzari, Comput. Phys. Commun. **185**, 2309 (2014).
[37] D. Hsieh, Y. Xia, L. Wray, D. Qian, A. Pal, J. H. Dil, J. Osterwalder, F. Meier, G. Bihlmayer, C. L. Kane, Y. S. Hor, R. J. Cava, and M. Z. Hasan, Science **323**, 919 (2009).
[38] N. B. Kopnin, T. T. Heikkilä, and G. E. Volovik, Phys. Rev. B **83**, 220503 (2011).
[39] E. Tang and L. Fu, Nat. Phys. **10**, 964 (2014).
[40] G. Z. Magda, X. Jin, I. Hagymasi, P. Vancso, Z. Osvath, P. Nemes-Incze, C. Hwang, L. P. Biro, and L. Tapaszto, Nature (London) **514**, 608 (2014).

[41] C. Webb and P. M. Williams, Phys. Rev. B **11**, 2082 (1975).
[42] A. H. Thompson, Phys. Rev. Lett. **34**, 520 (1975).
[43] H. E. Brauer, H. I. Starnberg, L. J. Holleboom, V. N. Strocov, and H. P. Hughes, Phys. Rev. B **58**, 10031 (1998).
[44] S. Cahangirov, M. Topsakal, E. Aktürk, H. Şahin, and S. Ciraci, Phys. Rev. Lett. **102**, 236804 (2009).
[45] E. Morosan, H. W. Zandbergen, B. S. Dennis, J. W. G. Bos, Y. Onose, T. Klimczuk, A. P. Ramirez, N. P. Ong, and R. J. Cava, Nat. Phys. **2**, 544 (2006).
[46] B. Sipos, A. F. Kusmartseva, A. Akrap, H. Berger, L. Ferró, and E. Tutiš, Nat. Mater. **7**, 960 (2008).
[47] A. F. Kusmartseva, B. Sipos, H. Berger, L. Forró, and E. Tutiš, Phys. Rev. Lett. **103**, 236401 (2009).
[48] T. Fukui and Y. Hatsugai, J. Phys. Soc. Jpn. **76**, 053702 (2007).
[49] A. A. Soluyanov and D. Vanderbilt, Phys. Rev. B **83**, 035108 (2011).
[50] Z. Ringel and Y. E. Kraus, Phys. Rev. B **83**, 245115 (2011).
[51] N. Marzari, A. A. Mostofi, J. R. Yates, I. Souza, and D. Vanderbilt, Rev. Mod. Phys. **84**, 1419 (2012).